

Controlling Electronic Access to the Spin Excitations of a Single Molecule in a Tunnel Junction

Ben Warner^{a,b}, Fadi El Hallak^{a,†}, Henning Prüser^a, Afolabi Ajibade^{a,b}, Tobias G. Gill^{a,c}, Andrew J. Fisher^{a,b}, Mats Persson^{d,e}, and Cyrus F. Hirjibehedin^{a,b,c,*}

^aLondon Centre for Nanotechnology, University College London (UCL), London WC1H 0AH, UK

^bDepartment of Physics & Astronomy, UCL, London WC1E 6BT, UK

^cDepartment of Chemistry, UCL, London WC1H 0AJ, UK

^dSurface Science Research Centre and Department of Chemistry, University of Liverpool, Liverpool, L69 3BX, UK

^eDepartment of Applied Physics, Chalmers University of Technology, SE-412 96, Göteborg, Sweden

*Email: c.hirjibehedin@ucl.ac.uk

[†]Present address: Seagate Technology, Derry BT48 0BF, UK

Methods

Scanning Tunnelling Microscopy

STM experiments were performed using an Omicron Cryogenic STM operating in ultrahigh vacuum (chamber pressures below 5×10^{-10} mbar) at a sample temperature of 2.5 K. Mechanically polished PtIr wires (Unisoku) wire used as STM tips, which were prepared by controlled mechanical indentation into the sample. Superconducting magnets were used to apply a magnetic field B of up to 6 T perpendicular to the surface of the sample.

The bias voltage V_b is always quoted in sample bias convention. Topographic images are obtained in the constant current imaging mode with V_b and tunnel current I set to V_{set} and I_{set} respectively. Differential conductance dI/dV measurements are obtained using a lock-in amplifier, with typical modulation voltages of 3 mV (0.05 mV) at ~ 737 Hz added to V_b for high voltage (low voltage) spectra. Spectra are acquired by initially setting $V_b=V_{set}$ and $I=I_{set}$, disabling the feedback loop, and then sweeping V_b while recording I and dI/dV . All of the electrical wires going into the STM are either filtered or grounded to reduce the impact of external high frequency electrical noise.

Cu(001) samples (MaTeck single crystal) were prepared by repeated cycles of sputtering with Ar while annealing to 500 °C. Cu₂N was prepared on top of clean Cu(001) samples by sputtering with N₂ and annealing to 350 °C. FePc molecules (Sigma Aldrich) were degassed at 375 °C before sublimating them from a crucible for 20 s at 350 °C on to a room-temperature sample.

Additional experimental data can be found online. See DOI: [10.6084/m9.figshare.c.3699211](https://doi.org/10.6084/m9.figshare.c.3699211).

Density Functional Theory

The electronic and geometric structure of FePc on Cu₂N/Cu(001) was investigated by density functional theory (DFT) calculations using the Vienna ab-initio simulation program (VASP)³⁷ in the same manner as in Ref. 28; details are repeated here for easy reference. The electron-ion-core interactions and the exchange-correlation effects were treated using the projected augmented wave (PAW) method,³⁸ with a plane-wave, kinetic energy cut-off of 400 eV, and the optB86B version of the van der Waals density functional,^{39,40,41,42} respectively. An intra-atomic Coulomb term U for the d -shell of the Fe atom was introduced according to Dudarev's scheme⁴³ and the self-consistent value of $U = 3.4$ eV, as obtained using the procedure proposed by Cococcioni and de Gironcoli,⁴⁴ was used. The Cu(001) surface is represented in a super-cell by a six layer slab with a c(12x12) surface unit cell and a 16.2 Å vacuum region. During the geometry optimization, the atoms in the bottom two layers were constrained at their bulk positions with a calculated lattice constant of 3.60 Å and the positions of the remaining atoms were relaxed until all forces were less than 0.02 eVÅ⁻¹.

The same super-cell was used for the isolated molecule. The Brillouin zone was sampled at the Γ point only.

The adsorbed molecule was found to retain a spin moment very close to $2 \mu_B$ ($S = 1$) and the adsorption energy was found to be weakly dependent on the azimuthal angle.²⁸ The DOS in Fig. 2 were obtained from the DOS of d partial waves around the Fe atom using the Fe-d projectors of the PAW. The local DOS in Fig. 3 were obtained from the calculated Kohn-Sham orbitals in the vacuum region about 3 Å from the surface.

Co-tunnelling Hamiltonian

We assume that direct tunnelling between the tip and the surface is supplemented by indirect tunnelling via the molecular site (MS). We compute the effect of the additional molecular state on the rates of both spin independent and dependent transport using a co-tunnelling model of spin-assisted transport. Following the method and the notation used in Delgado *et al.*²⁵, this transport model is obtained by applying second order perturbation theory to an effective low-energy co-tunnelling Hamiltonian.

The co-tunnelling Hamiltonian describes a two-step tunnelling process, where an electron tunnels onto the MS (from the tip or the surface electron reservoir) to form a charged intermediate state, and then tunnels off the MS into either reservoir (tip or surface). The energy of this charged intermediate state is assumed to be much larger than that of the tunnelling electrons, corresponding to off-resonant tunnelling or deep co-tunnelling. Here we treat the simplest case where there is a single orbital at the MS site and only singly negatively charged states will be considered (addition of one electron - we assume that the positively-charged hole states lie far from the Fermi energy).

Owing to the exchange coupling of the intermediate state to the spin moment of the MS, the initial and final states of the MS can have different spin states, which can cause a change of energy between the initial and final states of both the tunnelling electron and the MS. The spin states of the neutral molecule are given by eigenstates of an appropriate anisotropic spin-Hamiltonian for the phthalocyanine molecule:⁴⁵

$$H_0 = DS_{1z}^2 + E(S_{1x}^2 - S_{1y}^2)$$

For the transient negatively charged state produced by the addition of an electron, the Hamiltonian includes an exchange coupling J between the tunnelling electron with spin \mathbf{s}_2 and the localized MS spin \mathbf{S}_1 and an additional offset ΔE that represents other interactions, such as Coulomb interactions and the electron affinity of the MS orbital state:

$$H_{1e} = J(\mathbf{S}_1 \cdot \mathbf{s}_2) + DS_{1z}^2 + E(S_{1x}^2 - S_{1y}^2) + \Delta E$$

The values of D and E were taken from the fit of the data shown in Fig. S3, the charging energy ΔE is chosen such that the negatively-charged states are far enough away from the zero charge states to satisfy the co-tunnelling approximation, while J is adjusted to fit the heights of the inelastic tunnelling steps. From these equations the energy eigenvalues $E_{m,+}$ of H_{1e} and E_n of H_0 and the corresponding eigenstates $|m+\rangle$ and $|n\rangle$ can be determined.

The resulting co-tunnelling Hamiltonian that characterizes the perturbation on the effective Hamiltonian of the molecule is given by,

$$\mathcal{H}_{COTUN} = \hat{\mathcal{O}}_{\alpha\alpha'}^{(+)} f_{\alpha}^{\dagger} f_{\alpha'}$$

with

$$\hat{\mathcal{O}}_{\alpha\alpha'}^{(+)} = \sum_{\alpha, \alpha'} \sum_{\sigma, \sigma', n, n', m_{\pm}} \frac{V_{\alpha'}^* V_{\alpha}}{E_0 + \varepsilon_{\alpha} - E_{m_{\pm}}} \langle n | d_{\sigma} | m_{\pm} \rangle \langle m_{\pm} | d_{\sigma'}^{\dagger} | n' \rangle | n \rangle \langle n' |$$

Here d_{σ} and $d_{\sigma'}^{\dagger}$ are operators representing the destruction of an electron of spin σ and creation of an electron of spin σ' in the molecular orbital, while $\alpha \equiv \{k, \eta, \sigma\}$ is a combined notation for the electron momentum k , the reservoir index η (tip or surface) and electron spin σ ; f_{α} and f_{α}^{\dagger} are operators representing the destruction and creation of an electron in reservoir state α with energy ε_{α} respectively, while V_{α} is the hopping amplitude for an electron between the MS and state α . The energy gap between the neutral and charged states is characterized by the denominator $E_0 + \varepsilon_{\alpha} - E_{m_{\pm}}$; this gap depends strongly on the value of ΔE . Changing ΔE moves the density of charged states on the MS relative to the Fermi level of the electrode reservoirs.

The tunnelling rates between pairs of the neutral MS spin states ($|n\rangle$ and $|n'\rangle$) are found by applying Fermi's golden rule to the co-tunnelling Hamiltonian and assuming that the coupling strengths $V_{\alpha} \approx \bar{V}$ of the MS to the electrodes are independent of energy. We assume the co-tunnelling processes add incoherently to the direct tunnelling, which is itself independent of the MS. The rates of CT₁ (spin-independent) and CT₂ (spin-dependent) co-tunnelling processes can then be found (see Fig. 4). At $T = 0K$ and bias voltage V_b , the chemical potentials of tip and sample are related by $\mu_S - \mu_T = eV_b$ and we find

$$W^{nn'}(V_b) = \frac{2\pi}{\hbar} \int_{\mu_T}^{\mu_S} \sum_{\alpha, \alpha'} \left| \langle n | \hat{\mathcal{O}}_{\alpha\alpha'}^{(+)} | n' \rangle \right|^2 \delta(\varepsilon_{\alpha'} + \Delta_{nn'} - \varepsilon_{\alpha}) \delta(\varepsilon - \varepsilon_{\square}) d\varepsilon$$

where the spin excitation energy is

$$\Delta_{nn'} = E_n - E_{n'}$$

This results in a jump in the tunnelling rate

$$\Delta W^{nn'}(V_b) = \frac{2\pi}{\hbar} \rho_T \rho_S |\bar{V}|^4 \sum_{\sigma, \sigma'} \left| \sum_{m_{\pm}} \frac{\langle n | d_{\sigma} | m_{\pm} \rangle \langle m_{\pm} | d_{\sigma'}^{\dagger} | n' \rangle}{E_{m_{\pm}} - E_0 - \mu_T - V_b} \right|^2$$

whenever the potential difference between μ_T and μ_S is equal to the energy gap ($\Delta_{nn'}$) between two MS spin eigenstates, where ρ_T and ρ_S are the densities of states in the tip and surface respectively and are assumed to be constant with respect to energy in both the tip and the sample. Assuming that the spin is initially in its ground state ($n=0$), the CT₁ and CT₂ transport rates are then given by:

$$W_{CT1} = \Delta W^{00}$$

$$W_{CT2} = \sum_{n \neq 0} \Delta W^{n0}$$

Since

$$\sum_{m_{\pm}} \langle n | d_{\sigma} | m_{\pm} \rangle \langle m_{\pm} | d_{\sigma'}^{\dagger} | n' \rangle = \delta_{n, n'} \delta_{\sigma, \sigma'}$$

it follows that the CT_1 and CT_2 rates decay in different ways: W_{CT_1} decays as $(\Delta E)^{-2}$, while W_{CT_2} goes as $(\Delta E)^{-4}$ in the limit of large ΔE ($\Delta E \gg J, D$).

Figures

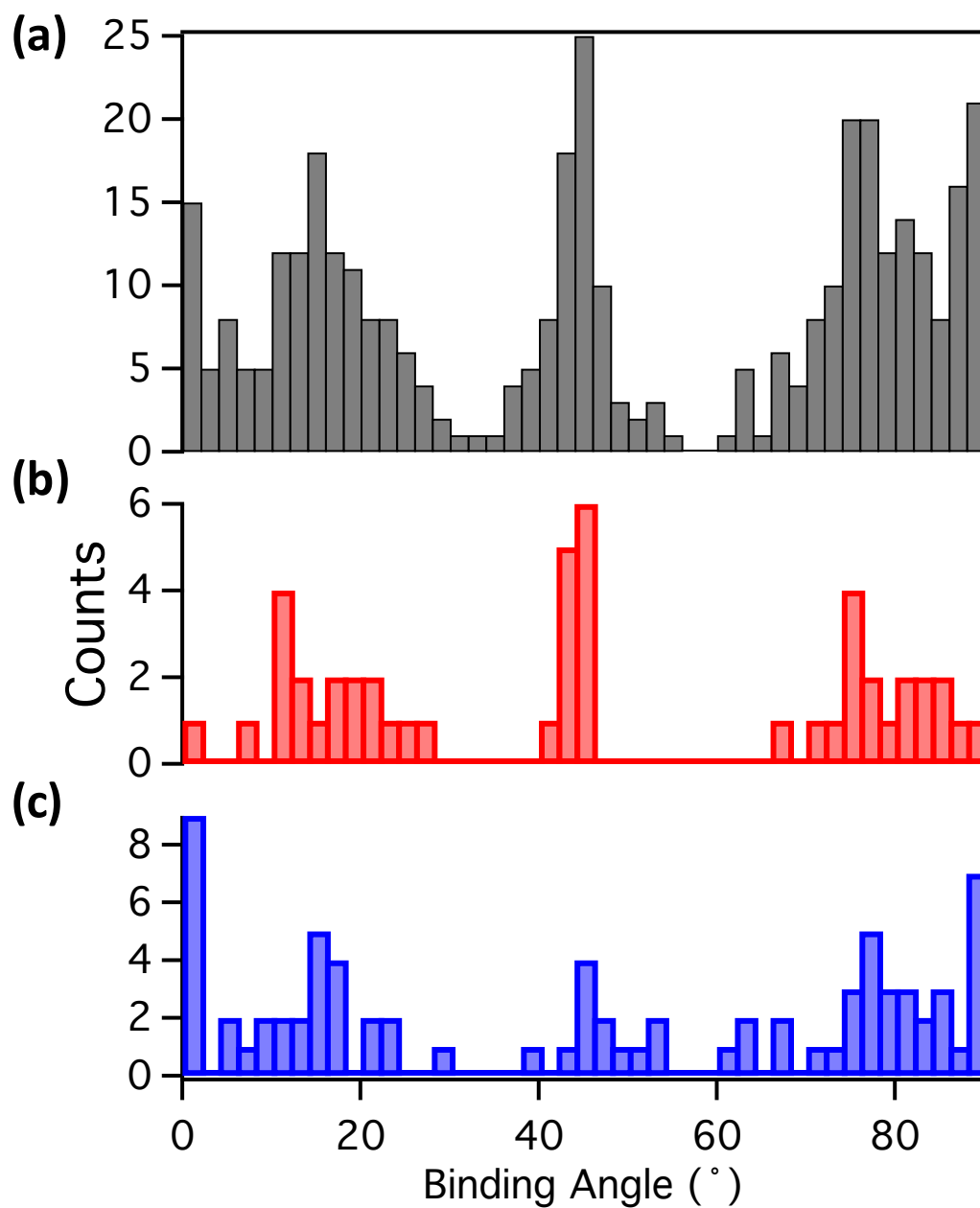


Figure S1. Binding angles of FePc on Cu₂N monolayer. (a) Black bars represent molecules on all binding sites. A wide range of binding angles is observed, with a preference for 0°, 18°, 45° with respect to the [100] axis of Cu. (b) Same as panel (a) for only FePc-Cu molecules. (c) Same as panel (a) for only FePc-N molecules.

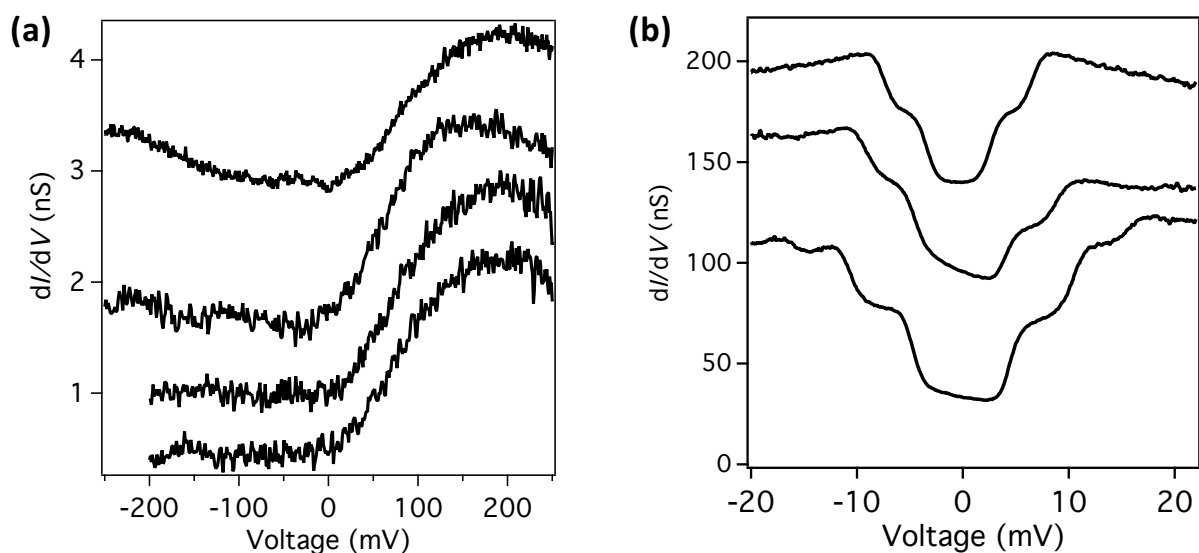


Figure S2. Variation in low bias spectroscopy for FePc on Cu_2N . (a) Low bias dI/dV spectroscopy over different FePc-Cu molecules shows little variation between different molecules. Spectra have been offset vertically for clarity. ($V_{set}=22-26$ mV, $I_{set}=1.5-2.0$ nA, $B=6.0$ T) (b) dI/dV spectroscopy measurements taken over different FePc-N molecules. IET steps are always observed. The three spectra shown here were chosen to highlight the variation observed in the number of steps, energy of the steps, and line shapes. Spectra have been offset for clarity. ($V_{set}=300-400$ mV, $I_{set}=0.5$ nA).

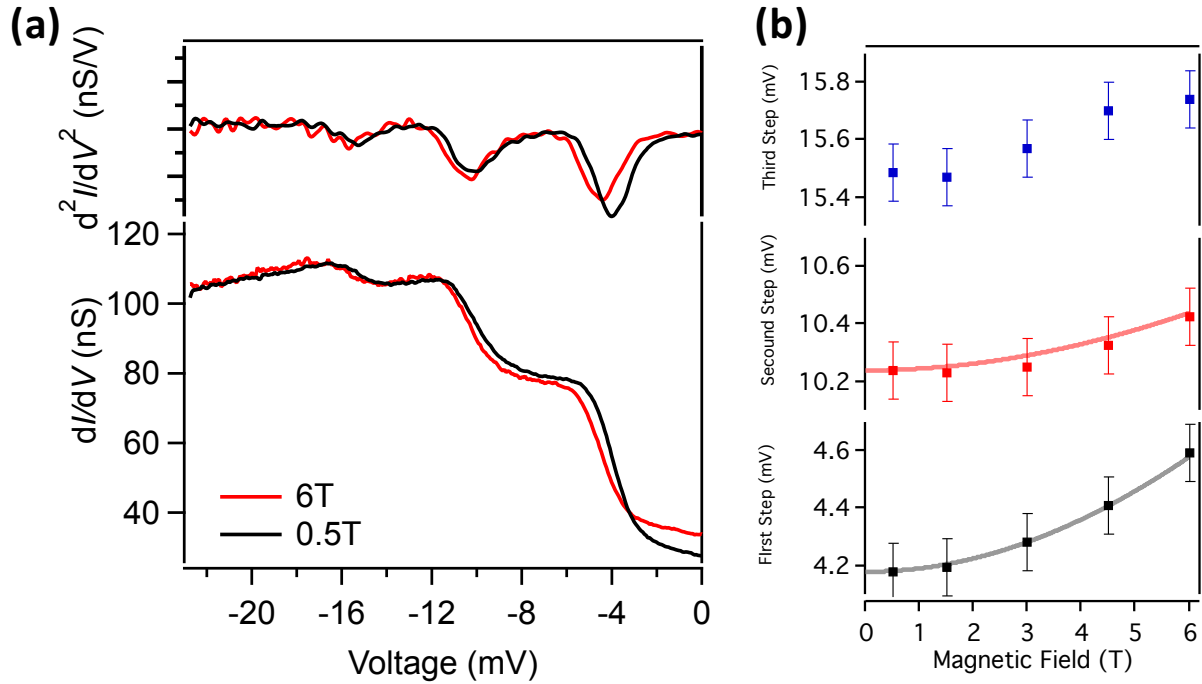


Figure S3. Magnetic field dependence of IET steps. (a) Low voltage dI/dV spectra and numerically differentiated d^2I/dV^2 spectra obtained over the centre of an Fe atom in FePc-N at 0.5T (black) and 6.0T (red) ($V_{set}=-22$ mV, $I_{set}=2$ nA). Small shifts are seen in the voltage of the centre of the steps, suggesting that the steps are related to magnetic excitations. (b) Step energy as a function of magnetic field. The energy of the step is observed to change with field. For the first and second steps, the expected change with magnetic field for an $S=1$ model ($g=2.69$) with axial anisotropy $D=-8.15$ meV and transverse anisotropy $E=2.09$ meV⁴⁵ has been added as a solid line. Data from this molecule is also shown in Fig. 1f.

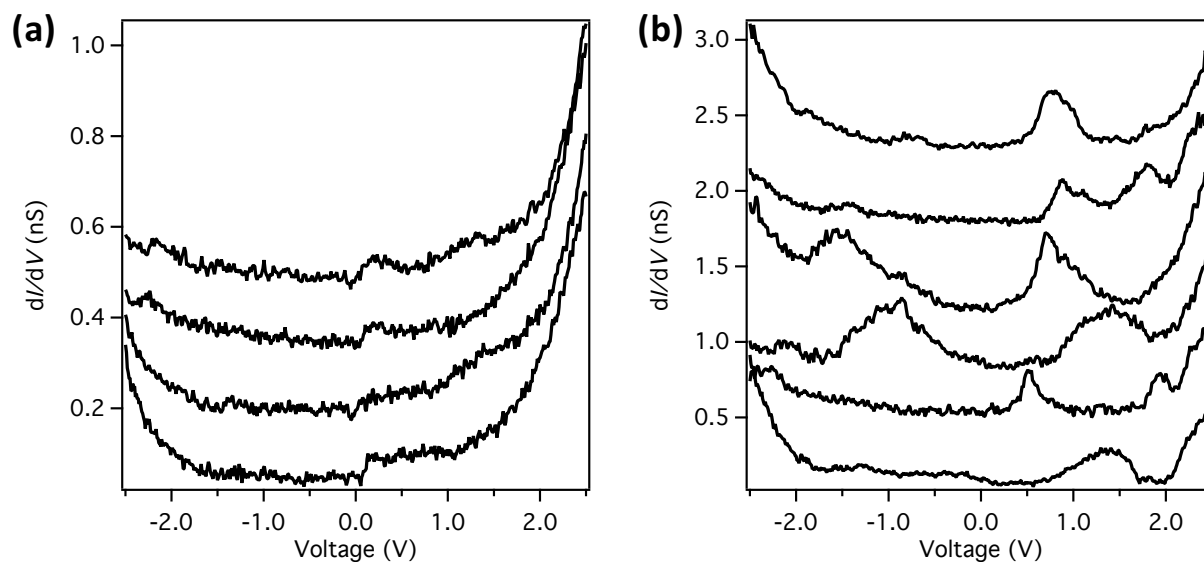


Figure S4. Variation in high voltage spectroscopy. (a) Spectra (offset vertically for clarity) acquired over the centre of FePc-Cu; little variation is observed. (b) Spectra (offset vertically for clarity) acquired over the centre of FePc-N; features are observed around +1.0 V and variations are observed between different molecules. Each spectrum is taken on a different molecule and in each panel the top spectrum is the one shown in Fig. 3 ($V_{set}=2.5$ V, $I_{set}=0.5$ nA).

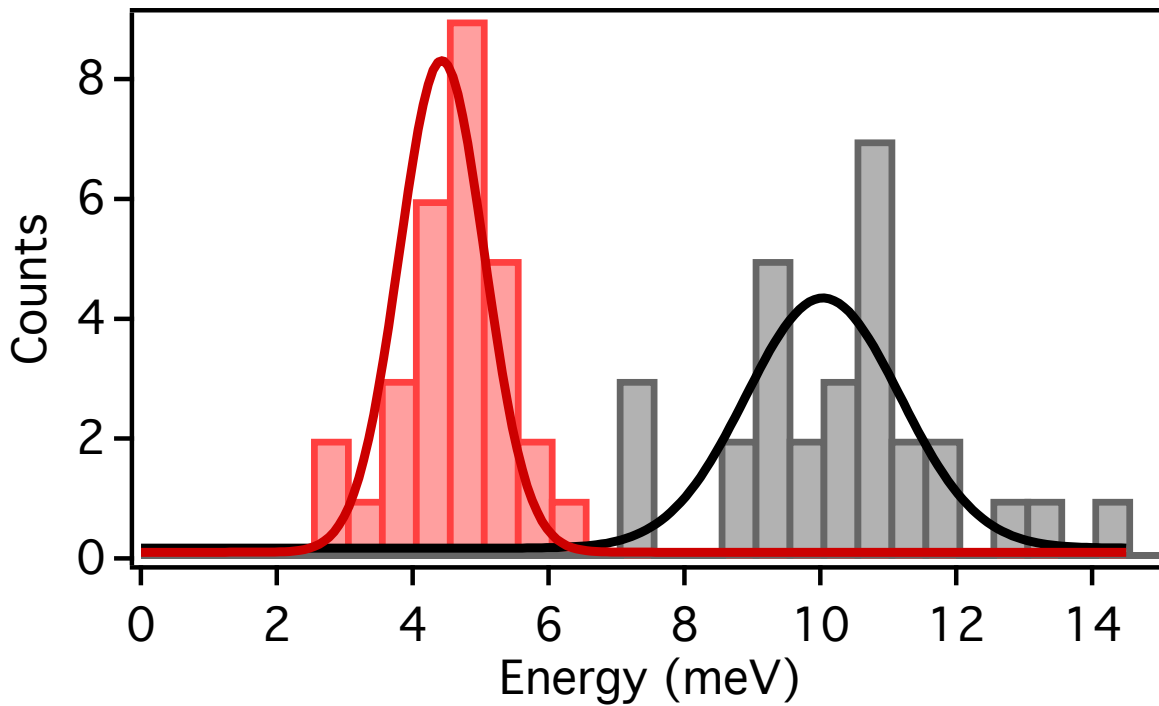


Figure S5. IET step energy distribution for FePc-N. Histogram of the IET step energy for the first (red) and second (grey) IET step observed on FePc-N. Thick lines represent Gaussian fits of the two distributions and have centres (widths) of 4.3 meV (0.9 meV) and 10.0 meV (1.6 meV) for the first and second step respectively.

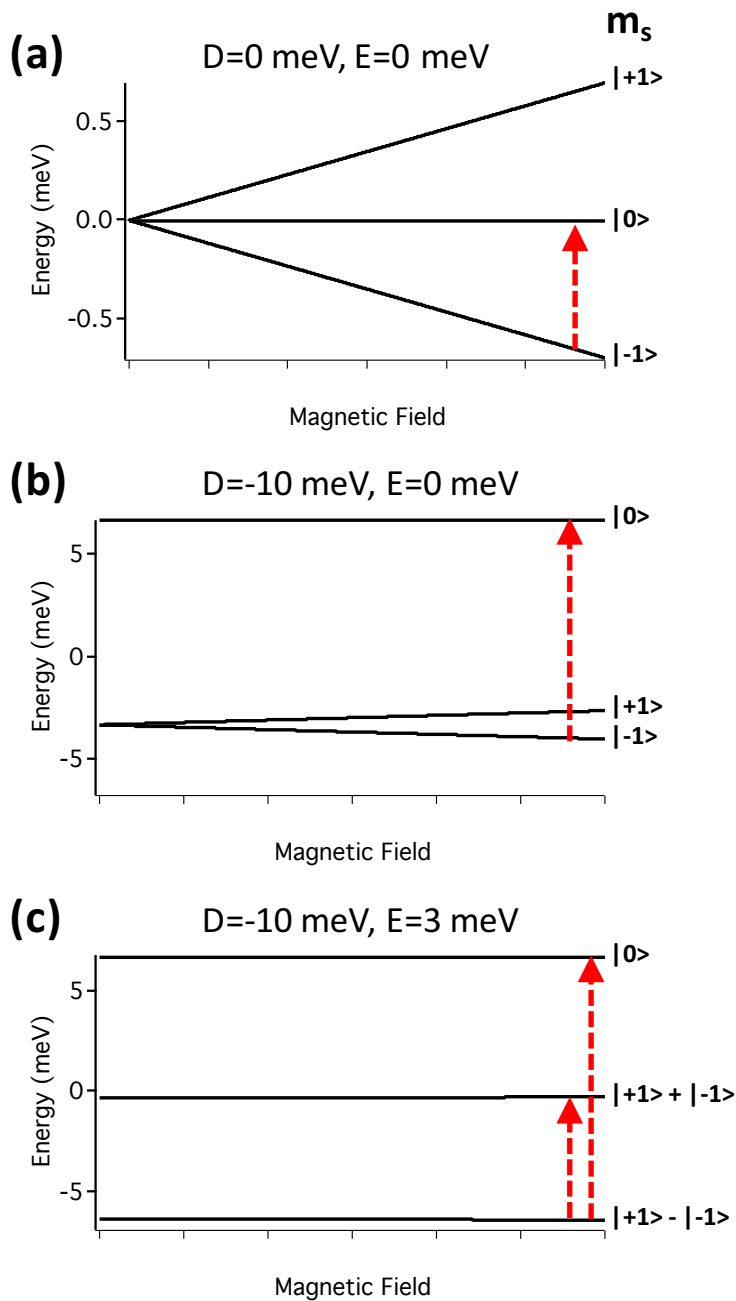


Figure S6. $S=1$ IET transitions. (a) Schematic level diagram for an $S=1$ system with $g=2$. Due to selection rules of $m_s=\pm 1$, only one transition from the ground state can occur (shown in red). (b) Axial anisotropy has been added, resulting in zero field splitting between the $S=\pm 1$ and $S=0$. Since $D=-10$ meV < 0 , the high spin state is the ground state. (c) Transverse anisotropy is added ($E=3$ meV), which mixes the $m_s=\pm 1$ states, and therefore a second transition from the ground state can occur.

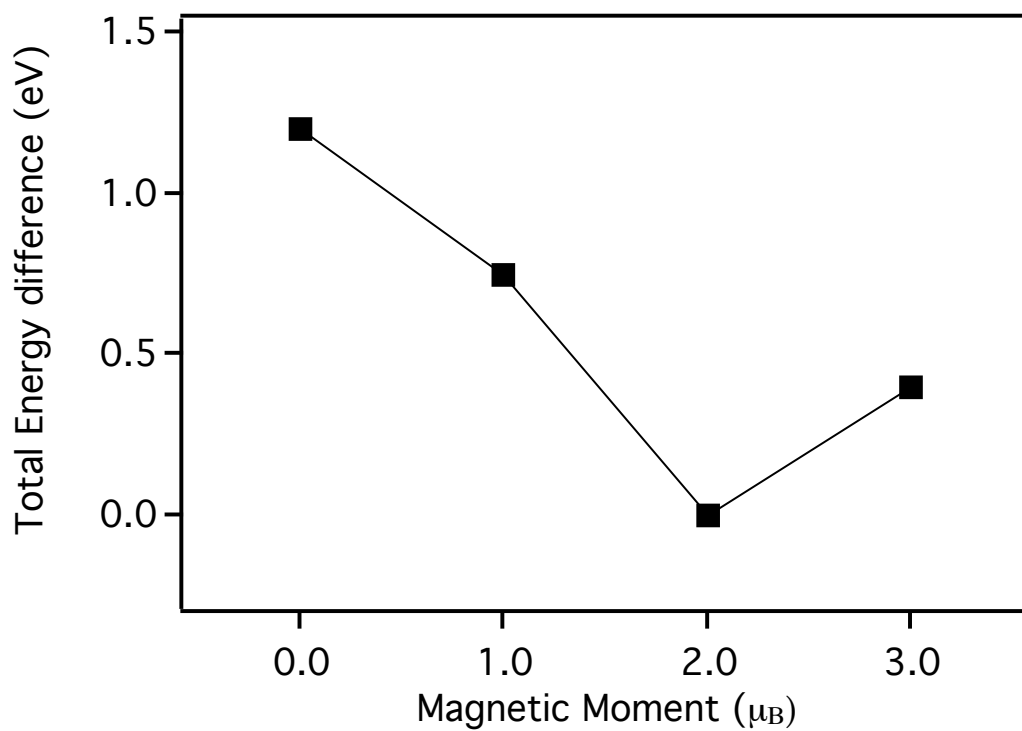


Figure S7. Energy vs. Magnetic Moment of an isolated FePc molecule. Relative total energies for magnetic moments $\mu \neq 2 \mu_B$ were obtained by constraining the difference between major and minor spin occupancies in the calculations.

Variations in IET spin excitations for FePc-N

As shown in Fig. S5, the energy of the IET steps for FePc-N shows notable variation in energy. Interestingly, we note that the distribution of the first step is smaller than the energy of the second step. Fitting a Gaussian to the histograms we observe that the first step is distributed around 4.3 meV, with a FWHM of 1.8 meV. The second step is distributed around 10.0 meV with a FWHM of 3.2 meV. The mean values are close to what is observed for FePc on CuO (4.1 meV, 9.0 meV).²⁰

The energy levels for a spin in an anisotropic environment can be described by the spin Hamiltonian:⁴⁵

$$H = DS_z^2 + E(S_x^2 - S_y^2)$$

A schematic diagram of an $S=1$ model with both transverse (D) and axial (E) anisotropy terms where the high spin state is the ground state (i.e. $D<0$) is shown in Fig. S6. The first IET step is the transition between antisymmetric and symmetric linear combinations of $m_z=\pm 1$ states. The energy of this step is defined by the transverse anisotropy, and we observe that this is very similar for FePc on CuO and Cu₂N. The second step is the transition from the $m_z=\pm 1$ states to the $m_z=0$ state. For FePc-N we observe that this step is higher in energy than on CuO, suggesting a slightly higher axial anisotropy. For Co on large islands of Cu₂N, the position of the Co on the island is observed to change the anisotropy;¹⁵ it is possible that a similar effect explains the greater distribution of the second step, though a systematic dependence on distance from the island edge has not been noted.

Interestingly, as seen in Fig. 1a, for some FePc-N molecules a third step is also observed. The first two steps appear at similar energies to FePc-N molecules that show only two steps, and fitting an $S=1$ model to the magnetic field dependence of these two steps gives a close match to the measured data. However, an $S=1$ model cannot account for the presence of the third step.

Because the third step appears at the same energy in both positive and negative bias, it is likely to be an IET transition. It is possible that it could be a vibrational mode; however as shown in Fig. S3, a small shift in the energy of the excitation is observed with applied magnetic field, suggesting that this step is also magnetic in character. Additionally, we observe that the spatial dependence of the third step is similar to that of the first and second, suggesting that it is created through the same process, or at least that its origin is related to the same molecular orbital.

For FePc, in which the magnetism arises from the d-shell, three spin excitations with non-zero intensity are only expected for $S=2$ ¹⁰ when considering the spin Hamiltonian above. Since the addition of an electron would only create a half-integer increase in spin, the most likely way for $S=2$ to occur is a reduction in the crystal field term. This effect has been observed for metal-porphyrins with axial ligands attached.⁴⁶ However the close match of the $S=1$ model with the first two steps, similarities with the FePc on CuO data, and the DFT calculations all suggest that FePc is $S=1$. One possible explanation for the a third IET transition that is magnetic in origin is an excitation to a different spin manifold.²³ However, DFT calculations where the spin moment is constrained suggest that, for the isolated FePc, configurations with $S\neq 1$ are more than a few hundred meV higher in energy (Fig. S7). Furthermore, the change in spin from calculations arose from a spin-polarization of the Cu substrate, and no change in the local Fe moment was observed.

Another explanation for the origin of the additional IET transition is an excitation related to the d-orbital moment of the Fe atom, which may not be quenched on top of a N atom because the N has four-fold symmetry in the surface. This would be consistent with the large g value observed in the magnetic field dependence, and similar excitations have been observed for Co atoms on top of O sites on MgO.¹⁶ Furthermore a large unquenched orbital moment has been observed for XMCD

measurements on FePc thin films.³³

References

- [37] G. Kresse and D. Joubert, *Phys. Rev. B*, 1999, **59**, 1758.
- [38] P. E. Blöchl, *Phys. Rev. B*, 1994, **50**, 17953.
- [39] M. Dion, H. Rydberg, E. Schröder, D. C. Langreth and B. I. Lundqvist, *Phys. Rev. Lett.*, 2004, **92**, 246401.
- [40] T. Thonhauser *et al.*, *Phys. Rev. B*, 2007, **76**, 125112.
- [41] G. Román-Pérez and J. M. Soler, *Phys. Rev. Lett.*, 2009, **103**, 096102.
- [42] J. Klimes, D. R. Bowler and A. Michaelides, *Phys. Rev. B*, 2011, **83**, 195131.
- [43] S. L. Dudarev, G. A. Botton, S. Y. Savrasov, C. J. Humphreys and A. P. Sutton, *Phys. Rev. B*, 1998, **57**, 1505.
- [44] M. Cococcioni and S. de Gironcoli, *Phys. Rev. B*, 2005, **71**, 035105.
- [45] D. Gatteschi, R. Sessoli and J. Villain, *Molecular Nanomagnets*, (Oxford Univ. Press, Oxford, 2006).
- [46] C. Wäckerlin *et al.*, *Angew. Chem. Int. Ed.*, 2013, **52**, 4568.